

## An investigation of PLA/W parts quality fabricated by FFF

Dimitrios Chaidas & John D. Kechagias

To cite this article: Dimitrios Chaidas & John D. Kechagias (2021): An investigation of PLA/W parts quality fabricated by FFF, Materials and Manufacturing Processes, DOI: [10.1080/10426914.2021.1944193](https://doi.org/10.1080/10426914.2021.1944193)

To link to this article: <https://doi.org/10.1080/10426914.2021.1944193>



Published online: 24 Jun 2021.



Submit your article to this journal 



Article views: 84



View related articles 



View Crossmark data 



# An investigation of PLA/W parts quality fabricated by FFF

Dimitrios Chaidas and John D. Kechagias

Design and Manufacturing Laboratory (DML), University of Thessaly, Karditsa, GR Greece

## ABSTRACT

Wood-flour PLA (PLA/W) composite material is a recyclable new material that is suitable for wood-looking components. This organic material can be found in different wood-flour (WF) compositions recently and is appropriate for the FFF (Fused Filament Fabrication) process. The current research investigates the impact of two key parameters, the nozzle temperature (NT, °C) and the layer thickness (LT, mm) onto surface quality (roughness average Ra and maximum profile height Rt; µm) and dimensional accuracy (linear external and wall thickness in X and Y direction, mm). A commercially available wood flour of pine with additives and pure PLA used for the experimental work. The results are analyzed using statistical descriptive tools (ANOM, ANOVA and interaction plots) and regression analysis for modeling the results. It has been found that lower values of LT and NT optimize both the surface quality and the dimensional accuracy. The LT is the dominant parameter for the surface quality, while both the LT and the NT are equally important for dimensional accuracy.

## ARTICLE HISTORY

Received 12 March 2021  
Accepted 13 June 2021

## KEYWORDS

PLA; wood; printing; surface; accuracy; temperature; thickness; ANOVA; ANOM

## Introduction

The fused filament fabrication (FFF) or 3D printing process creates objects layer-by-layer using digital CAD data.<sup>[1]</sup> Methods of 3D printing include FFF, photopolymerization, sheet lamination, powder bed fusion, etc.<sup>[2]</sup> The FFF process is used in various industries, such as aerospace, medical, architecture, industrial design, education, fashion industries, etc.<sup>[3]</sup> The FFF process has become popular nowadays for its simplicity, affordable price, minimal material waste and the plethora of available material.<sup>[4]</sup>

Surface quality (SQ) and dimensional accuracy (DA) are the main quality indicators of the printed objects in the manufacturing process.<sup>[5]</sup> The quality of these objects is influenced by the adhesion and fusion between the layers. To achieve the best-printed result, various machine and material parameters are used in the FFF process.<sup>[6]</sup> These parameters have an important impact on process efficiency.<sup>[7]</sup> Layer thickness, printing temperature, build orientation, printing speed, the number of shells and the infill pattern are some of the most common FFF parameters.<sup>[8]</sup>

During the FFF process, a digital model is converted to an actual object by a filament that passes through the nozzle of the 3D printer. Various thermoplastics are used as main materials (filaments). The most common filaments used in this process are thermoplastics materials (PLA, ABS, PCs, PEEK, PETG, TPU, etc.). Therefore, the development of new composite materials is an important topic in the 3D printing community.<sup>[9]</sup>

Wood flour (WF) is used as filler to the PLA to improve the composite's thermal properties and reduce the cost of materials.<sup>[10,11]</sup> Different types of flours affect the PLA/W composite properties. Usually, the addition of 20–50 wt% WF increases tensile, flexural, and GT temperature.<sup>[12]</sup> Huda et al.<sup>[13]</sup>

observed higher strength for PLA/W that reinforced with maple wood than for pure PLA. A previous study reported that the PLA/W materials could utilize in the production of FFF parts because of good adhesion between WF and PLA.<sup>[14,15]</sup>

Kariz et al.<sup>[16]</sup> examined the influence of WF ratios (10–50 wt%) in PLA/W filament on the printed items. The results showed that specimens made from filaments with higher wood content had higher moisture content, larger dimensional swelling, and lower modulus of elasticity. Kain et al.<sup>[17]</sup> investigated the impact of different deposition angles on printed items with PLA/W materials containing 15 wt% and 25 wt% and showed when fiber content increases, the strength increases.

Ayrlimis et al.<sup>[18]</sup> has studied the impact of LT on the water absorption (WA) and strength of PLA/W FFF items. The results showed that the WA of the specimens increasing by increasing the LT while the thickness swelling decreased. The strength of the parts is improved by decreasing the LT. When the LT increases, the cross-section porosity of the parts increases too. They have also found that by increasing the amount of WF (0 to 50 wt%), the SQ of the specimens is significantly increased.

Guessasma et al.<sup>[19]</sup> examined the strength of PLA/W items in different temperatures by setting the temperature range between 210 and 250 degrees. The tensile strength improved slightly when the NT was increased from 210 to 230 degrees. The results showed that NT above 230 degrees was not appropriate, as the wood particles degradation can influence the strength. Zandi et al.<sup>[20]</sup> investigated the impact of LH (layer height), ND (nozzle diameter), ID (infill density), and PV (printing velocity) on the strength of PLA/W specimens. The results showed that the LH was the most important variable on the strength, followed by the ND and ID, while the PV was not significant.

Concluding, the factors that affect the FFF-3D printed part surface quality (SQ) and dimensional accuracy (DA) are the

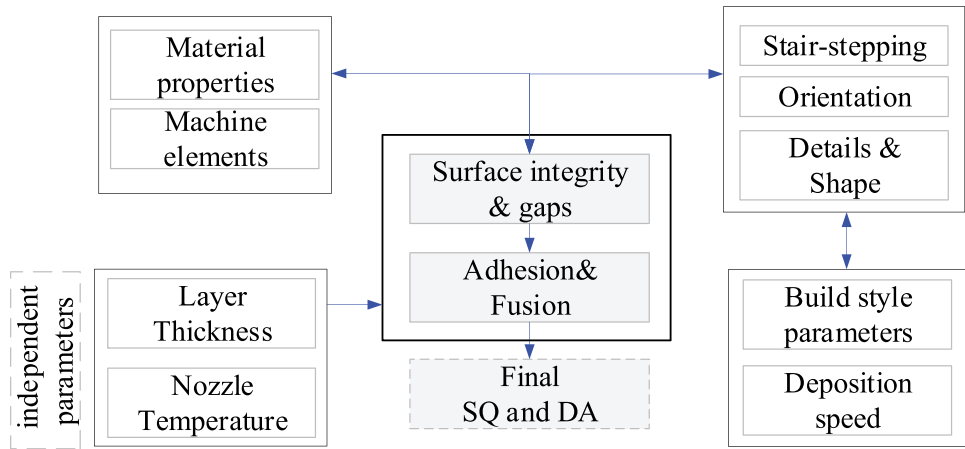


**Figure 1.** Factors that affect the SQ and DA of FFF parts.

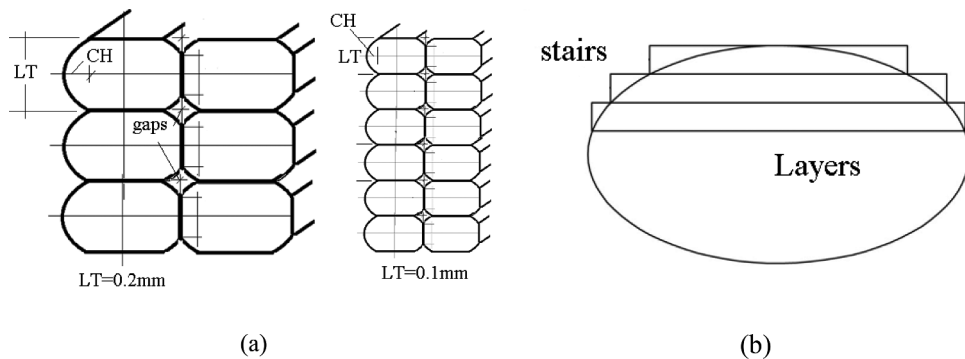


**Figure 2.** (a) Gaps between layers and (b) Stair-stepping phenomenon.

interlaminar adhesion and fusion (Fig. 1), which are affected by the surface integrity and material gaps (Fig. 2a). Layer thickness is the key factor for the surface integrity (stair-stepping phenomenon, Fig. 2b) and the nozzle temperature for the interlaminar bonding (gaps).

The above literature review demonstrates that many works have been conducted to investigate the influence of the FFF variables on the strength and water absorption of the PLA/W-FFF objects. Still, there is a gap in experimental work regarding their influence on the SQ and DA.

Therefore, the LT and NT are the two key parameters for quality control of the FFF process.<sup>[5]</sup> Hence, this work is an experimental investigation of how these two independent parameters influence the surface roughness ( $R_a$  and  $R_t$ ), and the accuracy of the linear external dimensions ( $DX$  and  $DY$ ) and the wall thickness ( $DWX$  and  $DWY$ ) of the PLA/W 3D-printed parts. The effects of the material composition, the machine elements design, the part orientation and shape, the built style parameters, and the printing speeds are not investigated.

## Materials and methods

### PLA/W parts

A thin-walled cuboid part ( $20 \times 23 \times 30$  across X, Y, and Z directions; mm) having a wall thickness of 2 mm was selected as the test part (see Fig. 3a). Craftbot Plus is used for printing

the specimens for this research (Fig. 3b). This printer has an aluminum platform, giving the ability to print with various materials. Its build space is  $250 \times 200 \times 200$  mm, the printing speed is up to 200 mm/s and the diameter of the nozzle 0.4 mm. The commercially fabricated PLA/W filament was used (NEEMA3D™ WOODPLUS; 30 wt% wood flour of pine and 70 wt% PLA; density 1.1–1.2 g/cm<sup>[3]</sup>; melting range 140–150°; diameter 1.75 mm).

### Design of experiments

The SQ and DA of the printed parts using the FFF process are affected by the parameter's values designated during this 3DP process (see Fig. 1). The process variables whose effects on the SQ and DA are investigated here are the NT and LT.

The weight (%) of the wood flour, the part shape and orientation, and the equipment control parameters characteristics (printing speeds, build parameters, etc.) are kept constant.

If the composition is changed, we will have different physical and thermal properties (range of melting point, transition temperature, viscosity index, etc.), affecting the interlaminar bonding conditions between the deposited layers. This is beyond the scope of this research, where a commercial material is used. For the same reasons, the part orientation, the part shape, and the printing conditions depending on machine characteristics are kept constant.

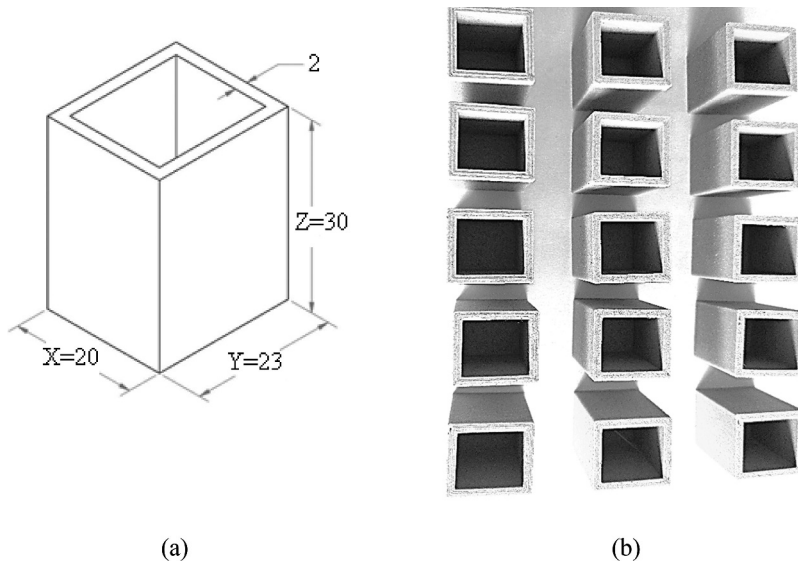


**Figure 3.** (a) Dimensions of the test part (b) PLA/W specimens.

**Table 1.** Selected FFF process parameters.

| Parameters  | Units   | Levels |     |     |     |     |
|---|---------|--------|-----|-----|-----|-----|
|   |         | 1      | 2   | 3   | 4   | 5   |
| <b>Variable parameters</b>  |         |        |     |     |     |     |
| Nozzle Temperature (NT)   | (°C)    | 180    | 190 | 200 | 210 | 220 |
| Layer Thickness (LT)  | (mm)    | 0.1    | 0.2 | 0.3 |     |     |
| <b>Constant parameters</b>  |         |        |     |     |     |     |
| Travel speed<br>(This speed occurs when 3D printer is not extruding material) | mm/s    |        |     | 40  |     |     |
| Infill printing speed   | mm/s    |        |     | 30  |     |     |
| Infill  | %       |        |     | 20  |     |     |
| Bed temperature   | °C      |        |     | 60  |     |     |
| Room temperature  | °C      |        |     | 20  |     |     |
| Room humidity   | %       |        |     | 50  |     |     |
| Outline/perimeter shells  | Number  |        |     | 4   |     |     |
| Raster angle  | Degrees |        |     | ±45 |     |     |
| Top solid layers  | Number  |        |     | 6   |     |     |
| Bottom solid layers   | Number  |        |     | 5   |     |     |

**Table 2.** Experimental array and measurements of the SQ and DA.

| No exp. | Parameters | Measurements |         |         |         |         |         |       |
|---------|------------|--------------|---------|---------|---------|---------|---------|-------|
|         |            | NT (°C)      | LT (mm) | Ra (µm) | Rt (µm) | DX (mm) | DY (mm) |       |
| 1       | 180        | 0.3          | 23.6    | 117.3   | 0.463   | 0.417   | 0.530   | 0.530 |
| 2       | 190        | 0.3          | 23.3    | 117.2   | 0.470   | 0.460   | 0.550   | 0.560 |
| 3       | 200        | 0.3          | 23.5    | 116.3   | 0.510   | 0.510   | 0.580   | 0.580 |
| 4       | 210        | 0.3          | 24.0    | 132.4   | 0.527   | 0.527   | 0.610   | 0.610 |
| 5       | 220        | 0.3          | 24.3    | 126.6   | 0.627   | 0.583   | 0.640   | 0.650 |
| 6       | 180        | 0.2          | 16.1    | 89.5    | 0.450   | 0.323   | 0.470   | 0.460 |
| 7       | 190        | 0.2          | 17.6    | 95.0    | 0.427   | 0.370   | 0.510   | 0.500 |
| 8       | 200        | 0.2          | 15.2    | 81.4    | 0.460   | 0.427   | 0.530   | 0.510 |
| 9       | 210        | 0.2          | 18.4    | 105.3   | 0.497   | 0.457   | 0.550   | 0.550 |
| 10      | 220        | 0.2          | 18.0    | 104.8   | 0.580   | 0.507   | 0.580   | 0.580 |
| 11      | 180        | 0.1          | 16.0    | 100.6   | 0.383   | 0.330   | 0.450   | 0.470 |
| 12      | 190        | 0.1          | 15.0    | 103.3   | 0.410   | 0.337   | 0.460   | 0.480 |
| 13      | 200        | 0.1          | 16.9    | 105.5   | 0.420   | 0.343   | 0.490   | 0.480 |
| 14      | 210        | 0.1          | 13.3    | 91.6    | 0.433   | 0.387   | 0.480   | 0.490 |
| 15      | 220        | 0.1          | 17.0    | 109.4   | 0.443   | 0.407   | 0.510   | 0.520 |
| Average |            |              | 18.8    | 106.4   | 0.473   | 0.426   | 0.529   | 0.531 |
| Min     |            |              | 13.3    | 81.4    | 0.383   | 0.323   | 0.450   | 0.460 |
| Max     |            |              | 24.3    | 132.4   | 0.627   | 0.583   | 0.640   | 0.650 |

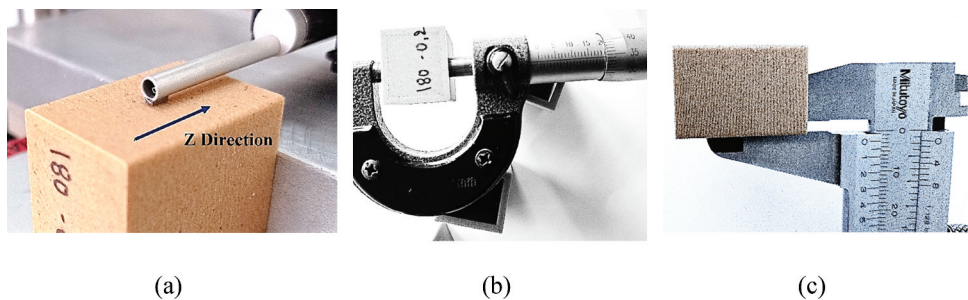


**Figure 4.** Measurements: (a) Surface roughness, (b) External dimensional accuracy and (c) Wall thickness.

The main concern of this research is to investigate the influence of two independent parameters, the LT, and NT, on the linear dimensions of a simple cuboid part and the surface quality of the vertical shell surfaces (Z direction measurements).

Table 1 summarizes the FFF process variables and their levels and the constant parameters used in this research. The variable process parameters are (i) The NT, nozzle temperature, and (ii) the LT that indicates the thickness of layers. Several process parameters, such as the raster angle, the base temperature, the number of shells and printing speeds were held constant throughout the FFF process.

A full factorial design has been selected, and an experimental table with all the combinations between the LT and NT has been used for the fabrication of the 15 specimens (Table 2).

During the SQ measurements, a DIAVITE profilometer is utilized (sample length/evaluation length: 0.8 mm/4 mm). A mean value of three reading is used in Z-direction (Fig. 4a). The SQ parameters measured during this study are the Ra and Rt. Ra ( $\mu\text{m}$ ) is the centerline average (CLA) roughness, while Rt ( $\mu\text{m}$ ) is the maximum height of the evaluation length profile.

A micrometer (0–25 mm; accuracy of 0.01 mm) is used for the DA linear external readings (Fig. 4b). Then the linear external differences DX and DY are calculated using the following equations:

$$D_X = \frac{X_{up} + X_{middle} + X_{down}}{3} - 20 \quad (1)$$

$$D_Y = \frac{Y_{up} + Y_{middle} + Y_{down}}{3} - 23 \quad (2)$$

where X and Y external dimensions are measured in three positions (upper, middle, and down), and the average value is calculated. Consequently, the nominal values are subtracted by the average values.

A Vernier caliper is utilized to measure the wall thickness in X and Y directions with a 0.05 mm accuracy (Fig. 4c). The wall differences in X and Y direction by the nominal wall thickness are abbreviated as DWX and DWY. All measurements are observed at 20 °C at room temperature.

## Results and discussion

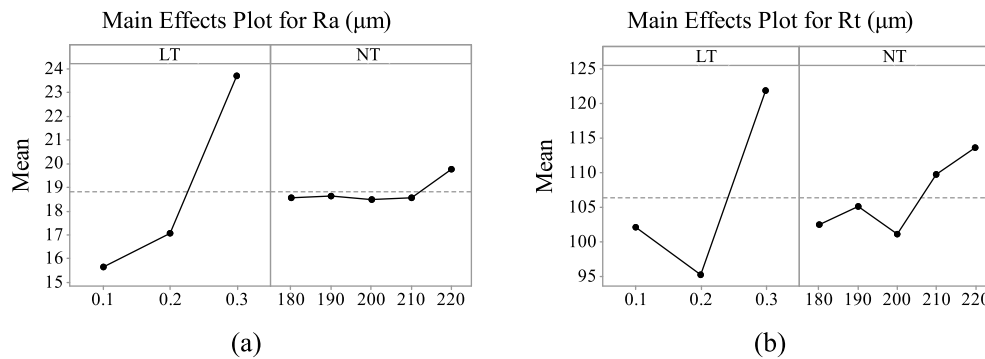
### Effects of the LT and NT on SQ

Both the Ra and Rt are very popular in characterizing manufactured surfaces and affecting the performance during the manufacturing components' assembly processes. Figure 5a and 5b show the influence of the NT and LT on the Ra and Rt during the 3D-printed specimens, respectively. At a glance, these two figures display that the spreads of the mean values are larger for the LT than NT.

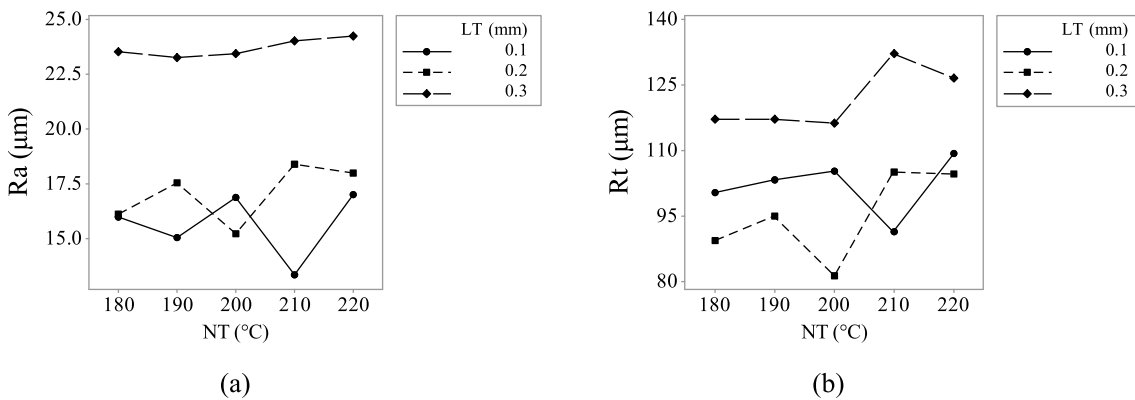
When the LT increases, both the Ra and Rt increase resulting in lower SQ. These increase in Ra and Rt values are expected following Fig. 2a. When the LT increases, the beds of the vertical shells become rougher with deeper grooves.

The NT affects slightly both the Ra and Rt. When the NT increases from 180 to 200 °C, the Ra and Rt decrease, becoming slightly better. Then from 200 to 220 °C, the Ra and Rt become gradually worse. The 200 °C optimize the surface integrity of the vertical shells resulting in better bonding with smaller valleys heights.

According to the Ra and Rt, how the LT and NT interact with each other can be shown in Fig. 6a and b, respectively.



**Figure 5.** MEP plots: (a) Ra (b) Rt.

**Figure 6.** Interaction plots: (a) Ra (b) Rt.**Table 3.** ANOVA analysis: Ra (μm) versus LT (mm); NT (°C).

| Source      | DF | Adj SS | Adj MS | F-Value | P-Value | %     |
|-------------|----|--------|--------|---------|---------|-------|
| LT (mm)     | 2  | 186.64 | 93.32  | 54.38   | 0.00    | 91.6  |
| NT (°C)     | 4  | 3.47   | 0.87   | 0.51    | 0.73    | 1.7   |
| Error       | 8  | 13.73  | 1.72   |         |         | 6.7   |
| Total       | 14 | 203.84 |        |         |         | 100.0 |
| R-sq        |    |        |        |         |         | 93.27 |
| R-sq (adj)  |    |        |        |         |         | 88.21 |
| R-sq (pred) |    |        |        |         |         | 76.32 |

**Table 7.** ANOVA analysis: DWX (mm) versus LT (mm); NT (°C).

| Source      | DF | Adj SS   | Adj MS   | F-Value | P-Value | %     |
|-------------|----|----------|----------|---------|---------|-------|
| LT (mm)     | 2  | 0.027053 | 0.013527 | 73.12   | 0.00    | 61.4  |
| NT (°C)     | 4  | 0.01556  | 0.00389  | 21.03   | 0.00    | 35.3  |
| Error       | 8  | 0.00148  | 0.000185 |         |         | 3.4   |
| Total       | 14 | 0.044093 |          |         |         | 100.0 |
| R-sq        |    |          |          |         |         | 96.64 |
| R-sq (adj)  |    |          |          |         |         | 94.13 |
| R-sq (pred) |    |          |          |         |         | 88.20 |

**Table 4.** ANOVA analysis: Rt (μm) versus LT (mm); NT (°C).

| Source      | DF | Adj SS | Adj MS | F-Value | P-Value | %     |
|-------------|----|--------|--------|---------|---------|-------|
| LT (mm)     | 2  | 1933.1 | 966.57 | 16.23   | 0.002   | 70.6  |
| NT (°C)     | 4  | 327.4  | 81.84  | 1.37    | 0.324   | 12.0  |
| Error       | 8  | 476.4  | 59.55  |         |         | 17.4  |
| Total       | 14 | 2736.9 |        |         |         | 100.0 |
| R-sq        |    |        |        |         |         | 82.59 |
| R-sq (adj)  |    |        |        |         |         | 69.54 |
| R-sq (pred) |    |        |        |         |         | 38.80 |

**Table 8.** ANOVA analysis: DWY (mm) versus LT (mm); NT (°C).

| Source      | DF | Adj SS   | Adj MS   | F-Value | P-Value | %     |
|-------------|----|----------|----------|---------|---------|-------|
| LT (mm)     | 2  | 0.024973 | 0.012487 | 43.56   | 0       | 57.3  |
| NT (°C)     | 4  | 0.016307 | 0.004077 | 14.22   | 0.001   | 37.4  |
| Error       | 8  | 0.002293 | 0.000287 |         |         | 5.3   |
| Total       | 14 | 0.043573 |          |         |         | 100.0 |
| R-sq        |    |          |          |         |         | 94.74 |
| R-sq (adj)  |    |          |          |         |         | 90.79 |
| R-sq (pred) |    |          |          |         |         | 81.50 |

**Table 5.** ANOVA analysis: DX (mm) versus LT (mm); NT (°C).

| Source      | DF | Adj SS   | Adj MS   | F-Value | P-Value | %     |
|-------------|----|----------|----------|---------|---------|-------|
| LT (mm)     | 2  | 0.026324 | 0.013162 | 17.46   | 0.001   | 43.8  |
| NT (°C)     | 4  | 0.027733 | 0.006933 | 9.2     | 0.004   | 46.2  |
| Error       | 8  | 0.006031 | 0.000754 |         |         | 10.0  |
| Total       | 14 | 0.060089 |          |         |         | 100.0 |
| R-sq        |    |          |          |         |         | 89.96 |
| R-sq (adj)  |    |          |          |         |         | 82.44 |
| R-sq (pred) |    |          |          |         |         | 64.71 |

**Table 6.** ANOVA analysis: DY (mm) versus LT (mm); NT (°C).

| Source      | DF | Adj SS   | Adj MS   | F-Value | P-Value | %     |
|-------------|----|----------|----------|---------|---------|-------|
| LT (mm)     | 2  | 0.048664 | 0.024332 | 45.43   | 0.00    | 53.9  |
| NT (°C)     | 4  | 0.037311 | 0.009328 | 17.42   | 0.001   | 41.3  |
| Error       | 8  | 0.004284 | 0.000536 |         |         | 4.7   |
| Total       | 14 | 0.090259 |          |         |         | 100.0 |
| R-sq        |    |          |          |         |         | 95.25 |
| R-sq (adj)  |    |          |          |         |         | 91.69 |
| R-sq (pred) |    |          |          |         |         | 83.31 |

Lines of 0.1 and 0.2 mm of the LT interact in a complex way (anti-synergistic interaction).

The analysis of variances or ANOVA analysis is used to identify the impact of each variable on the Ra and Rt parameters (Tables 3 and 4). A parameter is characterized as important if the F-value is higher than 4 or the P-value is lower than 0.05. The ANOVA analysis for both the Ra and Rt show similar results. The dominant parameter is the LT that has F-values higher than 4 and P-values lower than 0.05. Moreover, the NT is insignificant ( $F < 2$ , and  $P > .05$ ) for both the Ra and Rt.

The mathematical models used for the Ra and Rt ANOVA analysis were the linear regression models without interaction products (eq. 3 and 4).

$$Ra = 5.99 + 40.44LT + 0.0236T \pm e \quad (3)$$

$$Rt = 32.7 + 99.4LT + 0.269 \pm e \quad (4)$$

Ra's predicted R-sq(pred) is about 76% and is close to R-sq (93%). Notwithstanding, R-sq(pred) for Rt have a big difference with the R-sq (82% and 39%, respectively). This means that the Ra predictions will be more accurate than the Rt predictions.

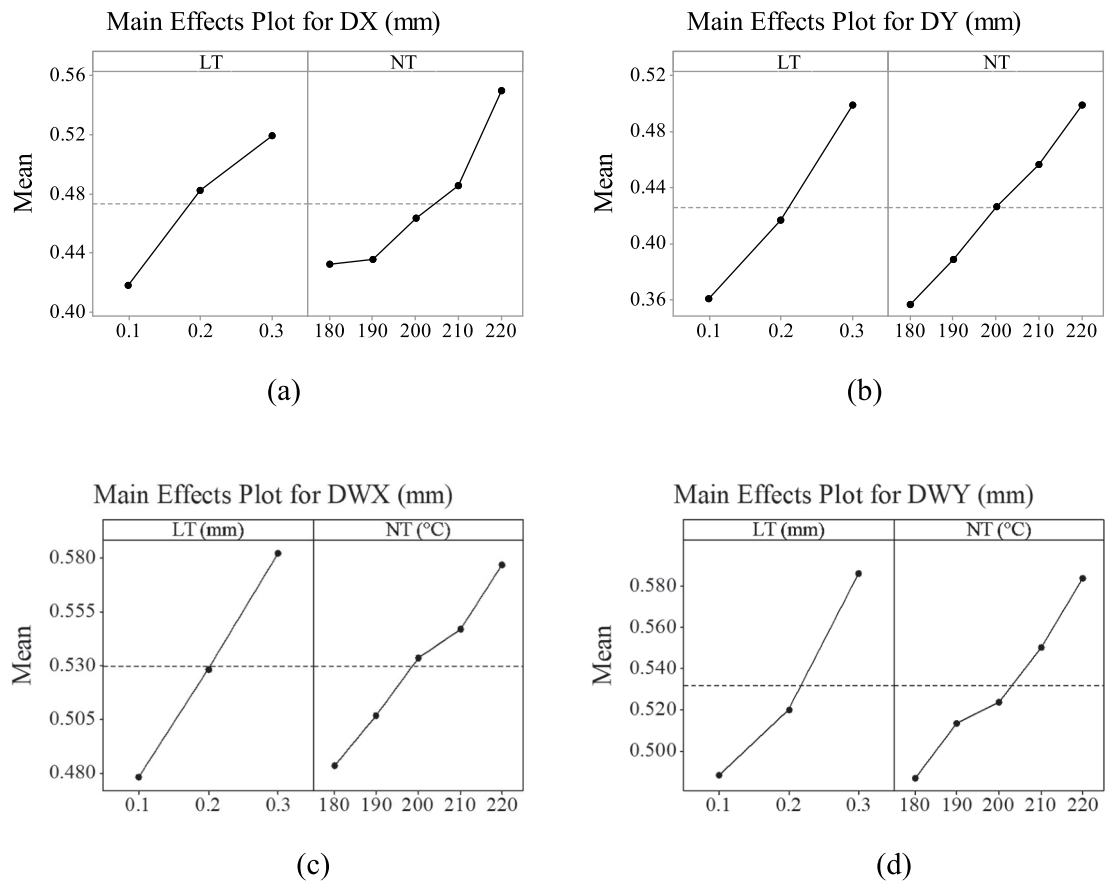


Figure 7. MEP plots: (a) DX, (b) DY, (c) DWX and (d) DWY.

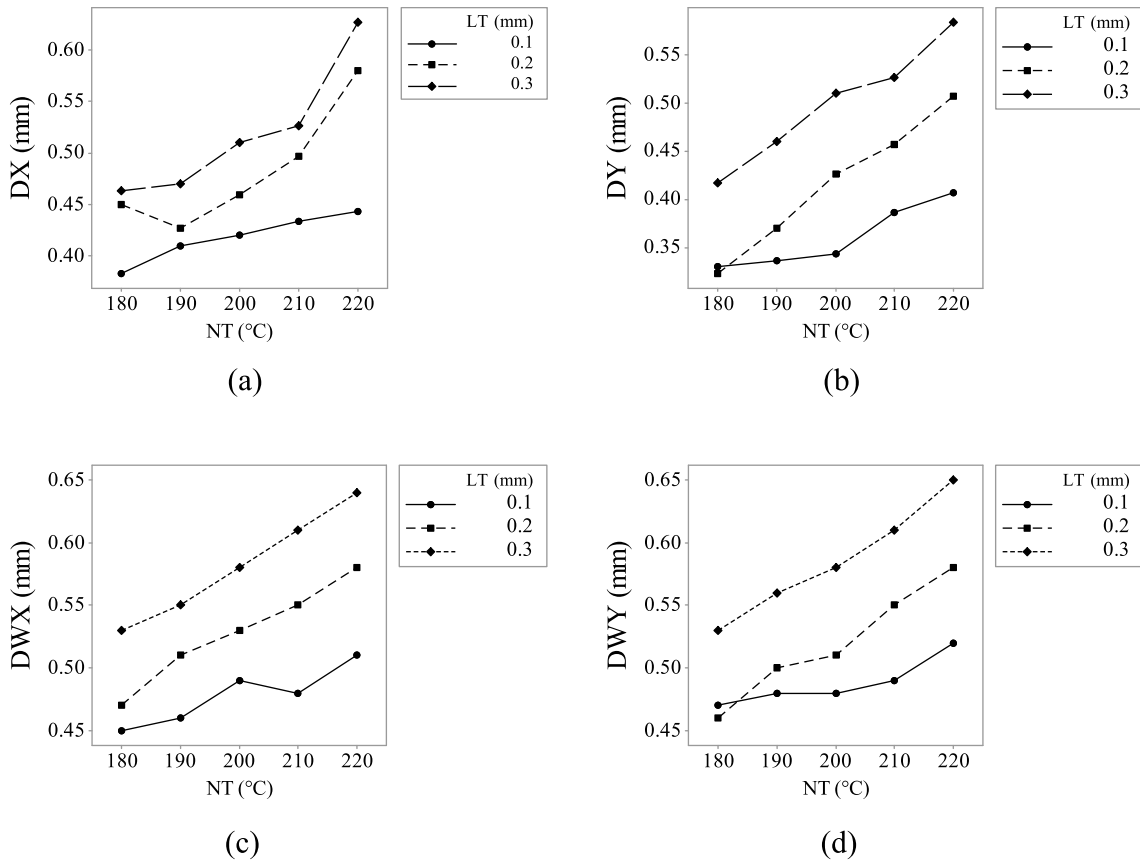
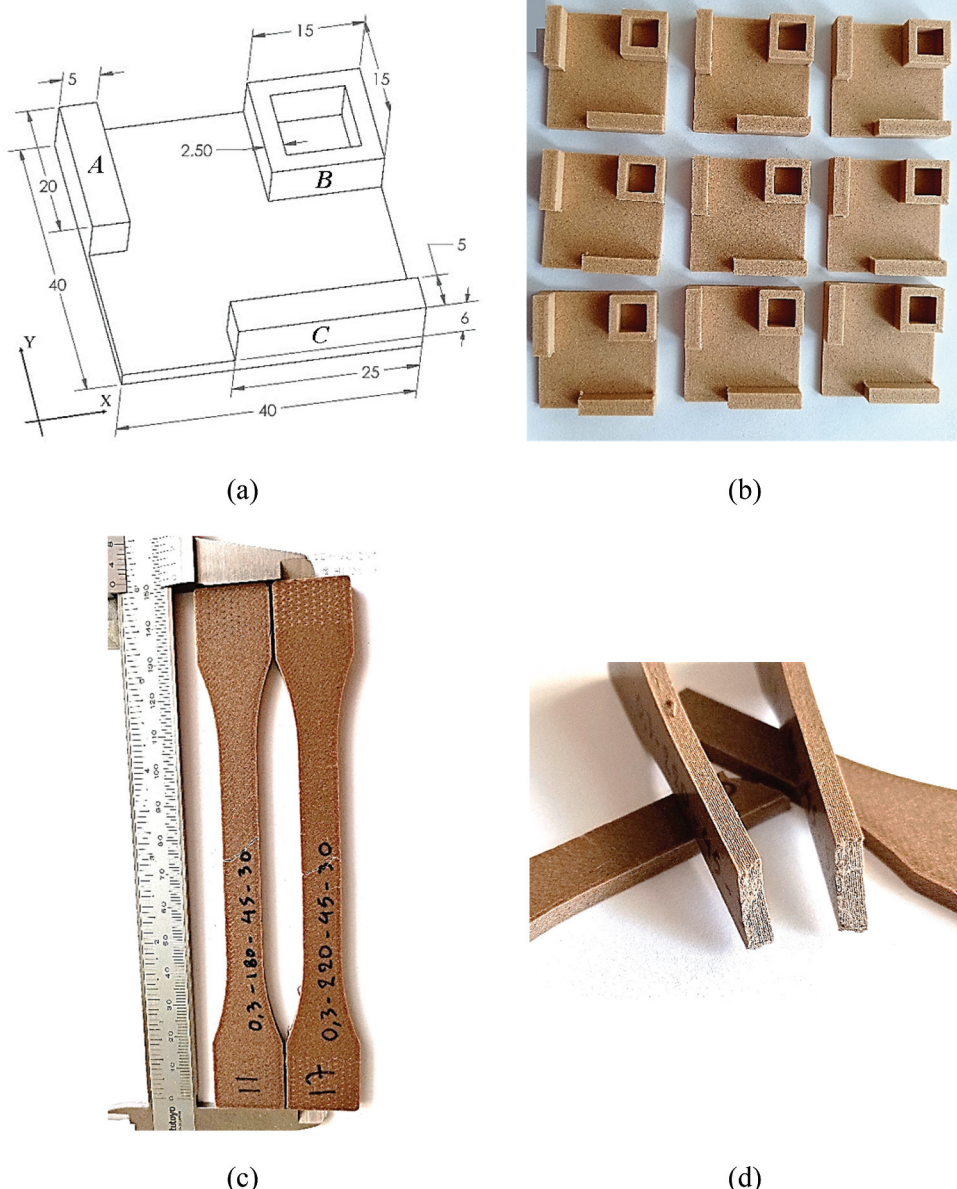


Figure 8. Interaction plots: (a) DX, (b) DY, (c) DWX and (d) DWY.



**Figure 9.** (a) Part used for validation experiment, (c) 3D printed parts ( $210^{\circ}\text{C}$  NT,  $0.1\text{ mm}$  LT), (c) Specimens used for bonding characterization ( $1\text{ mm/min}$  crosshead speed rate,  $45^{\circ}$  filament deposition angle,  $0.3\text{ mm}$  LT and  $180^{\circ}\text{C}$  NT) and (d) Broken specimens.

### Effects of the LT and NT on DA

The DA of the 3D-printed specimens is very significant for assemblies, especially for large parts to fit together.<sup>[7]</sup> All the deviation values (DX, DY, DWX, and DWY) of Table 2 have averaged between 0.426 and 0.531 mm. These values are very close to the nozzle diameter (0.4 mm) and are caused due to no nozzle compensation is used during the 3D Printing process. Tool compensation is a prevalent procedure that meets at machining processes.<sup>[21]</sup>

Figure 7a-d show the influence of the NT and LT on linear dimensional accuracy of the FFF process 3D-printed parts.

When the LT increases, all dimensional differences (DX, DY, DWX, and DWY) increase resulting in higher final dimensions. These increases in dimensions explained by Fig. 2a, where it is figured out that the chord height (CD) of the

filament beds is higher for  $0.2\text{ mm}$  than  $0.1\text{ mm}$  LT. Accordingly, higher temperatures increase the melted material viscosity, resulting in rougher deposited filament beds following the Ra and Rt values and higher final dimensions.

The LT and NT interaction charts versus the DX, DY, DWX, and DWY are displayed in Fig. 8a-d. It has been observed that the trend lines have similar directions. So, it can conclude that according to the bibliography, the linear regression models will be probably given adequate predictions.<sup>[22]</sup>

The ANOVA analysis is also used to identify the impact of each parameter on the DA measures (see [Tables 5–8]). On this occasion, the F-values are observed higher than 4 and P-values lower than 0.05. It is concluded that both the LT and NT parameters are significant for DA measures.

The mathematical models used for the DX, DY, DWX, and DWY ANOVA analysis were the linear regression models without interaction products (equations 5-8).

$$DX = -0.199 + 0.5067LT + 0.002856T \pm e \quad (5)$$

$$DY = -0.4176 + 0.6933LT + 0.003522T \pm e \quad (6)$$

$$DWX = -0.0280 + 0.5200LT + 0.002267T \pm e \quad (7)$$

$$DWY = -0.0267 + 0.4900LT + 0.002300T \pm e \quad (8)$$

The predicted R-sq(pred) and R-sq values are close for all the differences (DX, DY, DWX, and DWY). This means that the DX, DY, DWX, and DAY predictions are expected to be reliable for all DA attributes.

## **Evaluation experiments**

Following the above regression analysis, the proposed predictive models are validated by a new independent experiment using 0.1 mm LT and 210 °C NT. The model details and design are shown in Fig. 9a. The part built is 3D-printed nine times (Fig. 9b) by keeping all the printing parameters constant, at the same position on the platform. The observed surface roughness and dimensional readings are tabulated in Table 9.

It is shown in Table 9 that: (i) the Ra and Rt predictions are about -15.1% and -9.6% from the average of the nine repetitions (underestimated) and (ii) all DA attributes have an error ranged between -1.4 and +25.8% and (iii) the overall averages in the X and Y directions are 0.39 mm and 0.42 mm, having a small difference due to the statistical uncertainty.

Discrepancies (max-min values) of X and Y datasets are similar and about 0.12 and 0.11 mm.

Concerning the interlaminar bonding quality, two experiments in an Instron 3382 Universal Testing Machine are executed according to the ASTM D638 standards with a crosshead speed rate of 1 mm/min, 45° deposition angle rasters, 0.3 mm LT, and 180 °C NT (Fig. 9c). The specimens that have broken in the direction of the raster (45°) shown excellent interlaminar bonding (Fig. 9d).

## Conclusions

Concluding from the above experimental work, the SQ and DA of the PLA/W FFF parts are affected by the LT and NT.

The LT is very significant for the SQ parameters (Ra and Rt) and the DA parameters (DX, DY, DWX, and DWY). When the LT increases, both the SQ and DA parameters increase. The NT is not a significant factor for the SQ parameters (Ra and Rt) and significant for the DA parameters. When the NT increases, the Ra and Rt slightly increase after the 210 °C, while the DA increase significantly. All the Ra values ([Table 2](#)) were between 13 µm to 25 µm and the Rt between 81 µm to 132 µm ([Table 2](#)). These values are similar to those found in the bibliography for vertical surfaces of PLA-FFF parts.<sup>[7]</sup> Moreover, the DA shows a mean value of 0.49 mm for the all parameters, close to the nozzle diameter. This can be owed to nozzle compensation issues, as explained in the previous session “materials and methods”.

According to the ANOVA analysis, the LT is a significant parameter ( $F > 4$  and  $P < .05$ ) and affects both the SQ and the DA. The NT is an insignificant parameter for both the Ra and Rt ( $F < 2$  and  $P > .05$ ) and significant for all the DA parameters ( $F > 4$  and  $P < .05$ ). R-sq values imply that linear models are

**Table 9.** Validation experiment (0.1 mm LT and 210 °C): Ra, Rt, DX, and DY measurements.

| Surface quality (Measurements in Z Direction, $\mu\text{m}$ ) |      |       |       |       |      |       |       |       |       |         |                   |           |
|---|------|-------|-------|-------|------|-------|-------|-------|-------|---------|-------------------|-----------|
| No  | 1    | 2     | 3     | 4     | 5    | 6     | 7     | 8     | 9     | Average | Predicted         | error (%) |
| Ra  | 16.8 | 18.0  | 17.3  | 17.1  | 15.5 | 19.8  | 18.2  | 17.3  | 18.4  | 17.6    | 14.9 (Eq.3)       | -15.1     |
| Rt  | 97.0 | 109.2 | 123.6 | 109.1 | 96.5 | 111.0 | 109.0 | 124.6 | 106.4 | 109.6   | 99.1 (Eq. 4)      | -9.6      |
| DX-Dimensional Accuracy in X Direction (mm)                   |      |       |       |       |      |       |       |       |       |         |                   |           |
| No  | 1    | 2     | 3     | 4     | 5    | 6     | 7     | 8     | 9     | Average | Predicted (Eq. 5) | error (%) |
| DX-A1   | 0.44 | 0.45  | 0.44  | 0.45  | 0.44 | 0.44  | 0.44  | 0.45  | 0.44  | 0.44    | 0.45              | 1.8       |
| DX-A2   | 0.43 | 0.42  | 0.43  | 0.43  | 0.41 | 0.42  | 0.41  | 0.42  | 0.42  | 0.42    | 0.45              | 7.2       |
| DX-A3   | 0.42 | 0.42  | 0.42  | 0.43  | 0.42 | 0.41  | 0.40  | 0.41  | 0.42  | 0.42    | 0.45              | 8.3       |
| DX-B1   | 0.36 | 0.37  | 0.37  | 0.37  | 0.37 | 0.37  | 0.38  | 0.37  | 0.38  | 0.37    | 0.45              | 21.6      |
| DX-B2   | 0.36 | 0.35  | 0.36  | 0.35  | 0.36 | 0.36  | 0.37  | 0.35  | 0.37  | 0.36    | 0.45              | 25.8      |
| DX-B3   | 0.36 | 0.34  | 0.36  | 0.35  | 0.36 | 0.36  | 0.37  | 0.38  | 0.36  | 0.36    | 0.45              | 25.4      |
| DX-C  | 0.33 | 0.37  | 0.35  | 0.35  | 0.34 | 0.33  | 0.33  | 0.34  | 0.33  | 0.34    | 0.45              | 32.3      |

Min-Max = 0.12 mm Overall average = 0.39 mm

Nominal dimensions: X-A = 5 mm, X-B = 15 mm, X-C = 25 mm (see Figure 9a)

Min-Max = 0.11 mm Overall average = 0.42 mm

Nominal dimensions: Y-C = 5 mm, Y-B = 15 mm, Y-A = 20 mm (see Figure 9a)

suitable for the Ra, Rt, and DA parameter predictions (higher than 82.59%).

As future work, the authors suggest exploring more parameters of the 3D-printing FFF PLA/W process and shape evaluation (planarity, hole circularity, etc.) and IT grade characterization in optimized parameter levels for the 3D-printed specimens. The implementation of genetic algorithms and artificial neural networks are also proposed for more accurate predictions.

## ORCID

John D. Kechagias  <http://orcid.org/0000-0002-5768-4285>

## References

- [1] Jackiewicz, J., Manufacturing of Instructional Aids for Students at Low Cost by Means of 3D Printing. *Mater. Manuf. Processes.* **2017**, 32(10), 1116–1130. DOI: [10.1080/10426914.2016.1257135](https://doi.org/10.1080/10426914.2016.1257135).
- [2] Horn, T. J.; Harrysson, O. L., Overview of Current Additive Manufacturing Technologies and Selected Applications. *Sci. Prog.* **2012**, 95(3), 255–282. DOI:[10.3184/003685012X13420984463047](https://doi.org/10.3184/003685012X13420984463047).
- [3] Najmon, J. C.; Raeisi, S.; Tovar, A. 2 - Review of Additive Manufacturing Technologies and Applications in the Aerospace Industry. In *Additive Manufacturing for the Aerospace Industry*; Froes, F., Boyer, R., Eds. Elsevier: **2019**; pp 7–31. DOI: [10.1016/B978-0-12-814062-8.00002-9](https://doi.org/10.1016/B978-0-12-814062-8.00002-9).
- [4] Spoerk, M.; Gonzalez-Gutierrez, J.; Sapkota, J. Schuschnigg, S.; Holzer, C.; Effect of the Printing Bed Temperature on the Adhesion of Parts Produced by Fused Filament Fabrication. *Plast., Rubber Compos.* **2018**, 47(1), 17–24. DOI:[10.1080/14658011.2017.1399531](https://doi.org/10.1080/14658011.2017.1399531).
- [5] Turner, B. N.; Gold, S. A. A. Review of Melt Extrusion Additive Manufacturing Processes: II. Materials, Dimensional Accuracy, and Surface Roughness. *Rapid. Prototyp. J.* **2015**, 21(3), 250–261. DOI:[10.1108/RPJ-02-2013-0017](https://doi.org/10.1108/RPJ-02-2013-0017).
- [6] Chaidas, D.; Kitsakis, K.; Kechagias, J. Maropoulos, S. The Impact of Temperature Changing on Surface Roughness of FFF Process. *IOP Conf. Ser. Mater. Sci. Eng.* **2016**, 161, 012033. DOI: [10.1088/1757-899X/161/1/012033](https://doi.org/10.1088/1757-899X/161/1/012033).
- [7] Vyavahare, S.; Kumar, S.; Panghal, D. Experimental Study of Surface Roughness, Dimensional Accuracy and Time of Fabrication of Parts Produced by Fused Deposition Modelling. *Rapid. Prototyp. J.* **2020**, 26(9), 1535–1554. DOI:[10.1108/RPJ-12-2019-0315](https://doi.org/10.1108/RPJ-12-2019-0315).
- [8] Dey, A.; Yodo, N.; Systematic, A. Survey of FDM Process Parameter Optimization and Their Influence on Part Characteristics. *J. Manuf. Mater. Process.* **2019**, 3(3), 64. DOI: [10.3390/jmmp3030064](https://doi.org/10.3390/jmmp3030064).
- [9] Somireddy, M.; Singh, C.; Czekanski, A. Analysis of the Material Behavior of 3D Printed Laminates via FFF. *Exp. Mech.* **2019**, 59(6), 871–881. DOI: [10.1007/s11340-019-00511-5](https://doi.org/10.1007/s11340-019-00511-5).
- [10] Matuana, L.; Faruk, O. Effect of Gas Saturation Conditions on the Expansion Ratio of Microcellular Poly (Lactic Acid)/Wood-Flour Composites. *Express Polym. Lett.* **2010**, 4(10), 621–631. DOI: [10.3144/expresspolymlett.2010.77](https://doi.org/10.3144/expresspolymlett.2010.77).
- [11] Lv, S.; Gu, J.; Tan, H.; Zhang, Y. Modification of Wood Flour/PLA Composites by Reactive Extrusion with Maleic Anhydride. *J. Appl. Polym. Sci.* **2016**, 133(15), 1–9. DOI: [10.1002/app.43295](https://doi.org/10.1002/app.43295).
- [12] Meng, Q.; Hetzer, M.; De Kee, D. PLA/Clay/Wood Nanocomposites: Nanoclay Effects on Mechanical and Thermal Properties. *J. Compos. Mater.* **2011**, 45(10), 1145–1158. DOI: [10.1177/0021998310381541](https://doi.org/10.1177/0021998310381541).
- [13] Huda, M.; Drzal, L.; Misra, M.; Mohanty, A. Wood-Fiber-Reinforced Poly (Lactic Acid) Composites: Evaluation of the Physicomechanical and Morphological Properties. *J. Appl. Polym. Sci.* **2006**, 102(5), 4856–4869. DOI: [10.1002/app.24829](https://doi.org/10.1002/app.24829).
- [14] Wimmer, R.; Steyrer, B.; Woess, J.; Koddenberg, T.; Mundigler, N. 3D Printing and Wood. *Pro Ligno.* **2015**, 11(4), 144–149.
- [15] Faludi, G.; Dora, G.; Renner, K.; Móczó, J.; Improving Interfacial, P. B. Adhesion in PLA/Wood Biocomposites. *Compos. Sci. Technol.* **2013**, 89, 77–82. DOI: [10.1016/j.compscitech.2013.09.009](https://doi.org/10.1016/j.compscitech.2013.09.009).
- [16] Kariz, M.; Sernek, M.; Kuzman, M. K. Effect of Humidity on 3D-Printed Specimens from Wood-PLA Filaments. *Wood Res.* **2018**, 63(5), 917–922.
- [17] Kain, S.; Ecker, J.; Haider, A.; Musso, M. Petutschnigg, A. Effects of the Infill Pattern on Mechanical Properties of Fused Layer Modeling (FLM) 3D Printed Wood/Polylactic Acid (PLA) Composites. *Eur. J. Wood Wood Prod.* **2020**, 78(1), 65–74. DOI: [10.1007/s00107-019-01473-0](https://doi.org/10.1007/s00107-019-01473-0).
- [18] Ayrlilmis, N.; Kariž, M.; Kitek Kuzman, M. Effect of Wood Flour Content on Surface Properties of 3D Printed Materials Produced from Wood Flour/PLA Filament. *Int. J. Polym. Anal. Charact.* **2019**, 24(7), 659–666. DOI:[10.1080/1023666X.2019.1651547](https://doi.org/10.1080/1023666X.2019.1651547).
- [19] Guessasma, S.; Belhabib, S.; Nouri, H. Microstructure and Mechanical Performance of 3D Printed Wood-PLA/PHA Using Fused Deposition Modelling: Effect of Printing Temperature. *Polymers.* **2019**, 11(11), 1778. DOI: [10.3390/polym11111778](https://doi.org/10.3390/polym11111778).
- [20] Zandi, M. D.; Jerez-Mesa, R.; Lluma-Fuentes, J.; Roa, J. J.; Travieso-Rodriguez, J. A. Experimental Analysis of Manufacturing Parameters' Effect on the Flexural Properties of Wood-PLA Composite Parts Built through FFF. *Int. J. Adv. Manuf. Technol.* **2020**, 106(9–10), 3985–3998. DOI: [10.1007/s00170-019-04907-4](https://doi.org/10.1007/s00170-019-04907-4).
- [21] De Backer, J.; Christiansson, A. K.; Oqueka, J.; Bolmsjö, G. Investigation of Path Compensation Methods for Robotic Friction Stir Welding. *Ind. Robot. Int. J.* **2012**, 39(6), 601–608. DOI: [10.1108/01439911211268813](https://doi.org/10.1108/01439911211268813).
- [22] Phadke, M. S. *Quality Engineering Using Robust Design*; Englewood Cliffs, NJ: Prentice Hall, **1989**.